Sādhanā (2020)45:218
https://doi.org/10.1007/s12046-020-01457-4

A finite element prediction of first ply failure and delamination in composite conoidal shells using geometric nonlinearity

KAUSTAV BAKSHI[1,*] and DIPANKAR CHAKRAVORTY[2]

[1]Discipline of Civil Engineering, Indian Institute of Technology Indore, Indore 452020, India
[2]Department of Civil Engineering, Jadavpur University, Kolkata 700032, India
e-mail: bakshi.kaustav@gmail.com; Kaustav.bakshi@iiti.ac.in; prof.dipankar@gmail.com

MS received 15 April 2018; revised 20 March 2020; accepted 15 July 2020

Abstract. A review of the existing literature shows that there is only one research report available on failure of laminated composite conoidal shells using geometrically nonlinear strains. Thus, this paper aims for a detailed study on first ply failure and delamination predictions of laminated composite conoidal shell using von-Karman nonlinearity and first order shear deformation theory. The nonlinear equations are solved by Newton–Raphson iterative method. The failure loads of the shell are furnished for two different boundary conditions and stacking orders of cross and angle-ply laminations. The failure locations on the shell surface and failure modes/tendencies are also reported. This study finds that the SSCC boundary and 0°/90°/0° lamination should be selected by practicing engineers to achieve the maximum load carrying capacity of the conoid out of the two edge conditions considered here. Factor of safety values applicable on the failure loads are also suggested keeping due weightage to serviceability criterion.

Keywords. First ply failure; delamination; finite element formulation; conoidal shell; geometric nonlinearity.

1. Introduction

The laminated composite gained popularity in fabricating civil, aerospace and marine structures due to their high stiffness/strength to weight ratios, lesser thermal expansions and resistances against weathering actions. Moreover, the flexibility to tailor the stiffness and strength properties of the laminated composites by altering their fiber orientations and lamina stacking sequences made the material a lucrative option to the practicing engineers. The civil engineering industry utilizes the advantages of laminated composites and started to use laminated shell roofs to cover large unsupported areas which are found often in shopping malls, car parking lots, auditoriums and stadiums. The laminated shells are advantageous than the conventional reinforced concrete ones due to relatively lesser mass induced forces like seismic and foundation forces. Among the available shell forms, conoid enjoys special attention among civil engineers due to its doubly curved, aesthetically appealing, rigid and easy to fabricate surface. A number of researchers worked on different aspects of laminated conoidal shell structures. Das and Chakravorty [1, 2] worked on static bending of laminated conoids for different boundary conditions. The authors also [3, 4] reported fundamental frequencies and mode shapes of conoids. Kumari and Chakravorty [5, 6] worked on delaminated conoidal shells. However, the authors did not consider the onset of delamination. Nayak and Bandyopadhyay [7] studied forced vibration of isotropic conoids. Pradyumna and Bandyopadhyay [8, 9] worked on dynamic instability of conoids. Recently, a shear deformation model was proposed by Chaubey *et al* [10] for static analysis of moderately thick and deep laminated composite conoids. Hygrothermal analysis of laminated composite skew conoids was reported by Chaubey *et al* [11].

A laminated composite fails progressively as indicated by Singh and Kumar [12], Akhras and Li [13] and Ganesan and Liu [14]. The composite material may fail through first ply failure, where an individual lamina within the laminate fails first or through delamination, where two adjacent laminae separate from each other. First ply failure and delamination may initiate within the laminate and remain undetected and unprotected. The latent damage then progresses gradually within the laminate and it finally leads to total collapse of the shell roof under service condition. In order to prevent such catastrophe, a practicing engineer should know the load value at which such failures initiate in the laminate. Keeping the problem in mind, Reddy and Reddy [15] reported first ply failure loads of laminated

This paper is a revised and expanded version of an article presented in "First International Conference on Mechanical Engineering" held at 'Jadavpur University', Kolkata, India during January 4-6, 2018 (INCOM-2018.

*For correspondence
Published online: 31 August 2020

plates using geometrically linear and nonlinear strains. Kam *et al* [16] carried out experiments and reported the first ply failure loads of laminated plates. The authors adopted geometrically nonlinear finite element formulation and compared experimental and theoretical failure loads of the composite plates. First ply failure and onset of delamination for laminated composite plates were reported by Singh and Kumar [12]. Later Akhras and Li [13], Ganesan and Liu [14] and Lal *et al* [17] worked on first and progressive ply failures of laminated composite plates. Failure of composite shell panels was studied by few researchers recently but the authors adopted geometrically linear strains in their work. The first ply failure of singly curved and doubly curved shell panels were studied by Prusty *et al* [18]. Sengupta *et al* [19] worked on first and progressive ply failure of cylindrical shell roofs. Ghosh and Chakravorty [20] reported first and progressive failure of hypar shells. The authors [21] later reported first ply failure of spherical shell roofs. The first ply failure of laminated composite conoidal shells were studied by Bakshi and Chakravorty using geometrically linear strains [22]. Later the authors modified their finite element code and reported first ply failure of conoids using geometrically nonlinear strains [23].

The review of literature clearly shows that papers on failure study of composite shells are really scanty. There is only one research paper reporting first ply failure of laminated conoids using geometrically nonlinear strains. Thus, the authors aim for a detailed study on failure of laminated composite conoidal shell roofs. The novelties of the present paper in relation to the previous one is the failure loads of the laminated conoid for CCSS and SSCC boundary conditions, the prediction of failure modes using nonlinear strains and the delamination prediction model which were not a part of the previous paper reporting failure of conoids using nonlinear strains. The present paper studies failure of conoids subjected to concentrated load at the centre. First ply failure and delamination of the shell are studied in this paper. This paper concludes with meaningful design guidelines for practicing civil engineers which are framed considering the serviceability requirement also.

2. Problem formulation

A laminated composite conoidal shell (Figure 1) having radii of curvatures R_{yy} and R_{xy} is considered here. The material is assumed as linearly elastic and of uniform thickness 'h'. The thickness may consist of any number of thin laminae oriented at an angle 'θ' with reference to the global x-axis (Figure 1). The x and y axes are taken at the mid-surface of the shell having sides a and b, respectively.

An isoparametric finite element code formulated using eight noded doubly curved element (Figure 2) with C° continuity is used here. Five degrees of freedom are

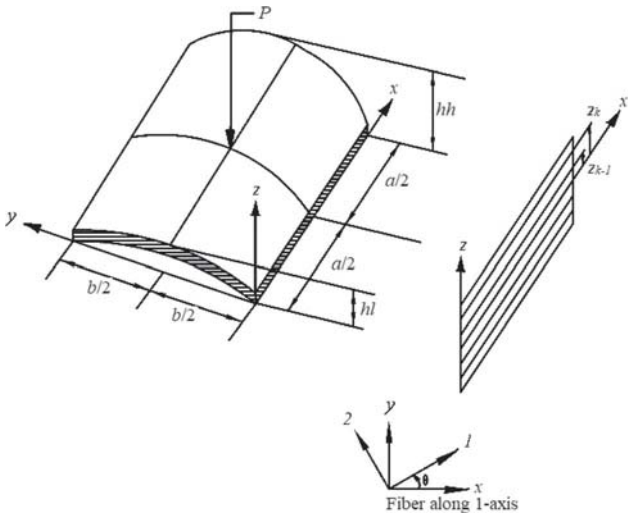

Figure 1. The conoidal shell.

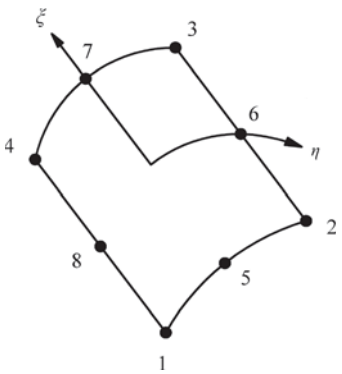

Figure 2. The eight noded shell element in natural co-ordinate system.

considered at each node of the element. The degrees of freedom are u, v, and w along x, y, z axes of the shell and α, β about y, x axes of the conoid.

The mid-surface strain vector $\{\varepsilon\}$ of the conoidal shell is expressed in Eq. (1) following von-Karman assumptions and Sanders' nonlinear strain-displacement relations [24].

$$\{\varepsilon\} = \{\varepsilon\}^{L} + \{\varepsilon\}^{NL} \tag{1}$$

where

$$\{\varepsilon\} = \left\{\varepsilon_x^0 \quad \varepsilon_y^0 \quad \gamma_{xy}^0 \quad k_x \quad k_y \quad k_{xy} \quad \gamma_{xz}^0 \quad \gamma_{yz}^0\right\}^T$$

$$\text{Linear mid - surface strains,} \quad \{\varepsilon\}^{L} = [B]^{L}\{d\} \tag{2}$$

$$\text{Nonlinear mid - srface strains,} \quad \{\varepsilon\}^{NL} = [B]^{NL}\{d\} \tag{3}$$

The mid-surface displacements of the shell is,

$$\{d\} = \{u \;\; v \;\; w \;\; \alpha \;\; \beta\}^T \tag{4}$$

$[B]^L$ denotes the linear strain-displacement matrix and is adopted here from Das and Chakravorty [1]. The nonlinear strain-displacement matrix $[B]^{NL}$ is given as follows:

$$[B]^{NL} = [A][G] \tag{5}$$

where

$$[A] = \begin{bmatrix} \frac{\partial w_0}{\partial x} & 0 \\ 0 & \frac{\partial w_0}{\partial y} - \frac{v}{R_{yy}} \\ \frac{\partial w_0}{\partial y} - \frac{v}{R_{yy}} & \frac{\partial w_0}{\partial x} \end{bmatrix}$$

$$[G] = \begin{bmatrix} 0 & 0 & \frac{\partial N_i}{\partial x} & 0 & 0 \\ 0 & -\frac{N_i}{R_{yy}} & \frac{\partial N_i}{\partial y} & 0 & 0 \end{bmatrix}$$

N_i = Shape function for i^{th} node of the element [1].

The governing differential equation of the composite shell is derived based on minimization of its total potential energy (π).

$$\pi = \frac{1}{2}\int_{v'} \{\varepsilon\}^T\{\sigma\}dv' - \int\int_A \{d\}^T\{q\}\,dA \tag{6}$$

'v'' and 'A' denote volume and area of the shell, respectively. To minimize total potential energy of the shell with respect to its deformations, it has to satisfy the following condition,

$$\frac{\partial \pi}{\partial\{d\}} = \psi \tag{7}$$

$$\frac{\partial}{\partial\{d\}}\iint_{v'} \{\varepsilon\}^T\{\sigma\}dv - \frac{\partial}{\partial\{d\}}\int\int_A \{d\}^T\{q\}\,dA = \psi \tag{8}$$

'Ψ' indicates residual of unbalanced forces. The Newton–Raphson approach is adopted here to minimize the residual force. At the end of the iterations the shell follows the equilibrium condition i.e. $\Psi = 0$.

The constitutive relationship of the shell is,

$$\{F\} = [D]\left(\{\varepsilon\}^L + \{\varepsilon\}^{NL}\right) \tag{9}$$

where

$$\{F\} = \int_{-h/2}^{+h/2} \{\sigma_x \quad \sigma_y \quad \tau_{xy} \quad \sigma_x.z \quad \sigma_y.z \quad \tau_{xy}.z \quad \tau_{xz} \quad \tau_{yz}\}^T dz.$$

The constitutive relationship matrix $[D]$ is the same in this study as it was reported by Das and Chakravorty [1].

Eq. (8) can be written as,

$$\sum_{i=1}^{ne}\psi_i = \sum_{i=1}^{ne}\left(\iint_A \frac{\partial\{\varepsilon\}^T}{\partial\{d\}}[D]\{\varepsilon\}dxdy - \sum_{i=1}^{8}\int\int_A \{N_i\}^T\{q\}dxdy\right)_i \tag{10}$$

$$\sum_{i=1}^{ne}\psi_i = \sum_{i=1}^{ne}\left(\iint_A [\bar{B}]^T[D]\{\varepsilon\}dxdy - \{Q\}\right)_i \tag{11}$$

where

$$[\bar{B}] = \frac{\partial\{\varepsilon\}^T}{\partial\{d\}} = [B]^L + [B]^{NL} \text{ and}$$

$$\{Q\} = \sum_{i=1}^{8}\int\int_A [N_i]^T\{q\}dxdy$$

Eq. (11) is solved by Newton-Raphson iteration method [25].

The tangent stiffness matrix ($[K_T] = \frac{\partial\{\psi(d_n)\}}{\partial\{d\}}$) is given as follows:

$$[K_T]_n = [K_L] + [K_Q]_n + [K_\sigma]_n \tag{12}$$

$$[K_L] = \iint_A \left([B]^L\right)^T[D][B]^L dxdy \tag{13}$$

$$[K_Q] = \iint_A \left([B]^L\right)^T[D][B]^{NL}dxdy + \iint_A \left([B]^{NL}\right)^T[D][B]^L dxdy + \iint_A \left([B]^{NL}\right)^T[D][B]^{NL}dxdydy \tag{14}$$

$$[K_\sigma]_n = \iint_A [G]_n^T\begin{bmatrix} N_1 & N_6 \\ N_6 & N_2 \end{bmatrix}[G]_n dxdy \tag{15}$$

N_1, N_2 and N_6 are inplane stress resultants [1].

$$[K_s]_n = \iint_A \left([B]^L\right)^T[D][B]^L dxdy + \frac{1}{2}\iint_A \left([B]^L\right)^T[D][B]_n^{NL}dxdy + \iint_A \left([B]_n^{NL}\right)^T[D][B]^L dxdy + \frac{1}{2}\iint_A \left([B]_n^{NL}\right)^T[D][B]_n^{NL}dxdydy$$

The stiffness matrices $[K_T]$, $[K_s]$ and the external load vector $\{Q\}$ are calculated by numerical integration method

using 2 × 2 Gauss quadrature rule. The iteration process is terminated when the following condition is satisfied.

$$\frac{\left(\{\psi\}^T\{\psi\}\right)^{1/2}}{\left(\{Q\}^T\{Q\}\right)^{1/2}} \times 100 \leq \text{Tolerance} \tag{16}$$

2.1 *First ply failure prediction*

The converged displacements of the conoidal shell are used to predict the lamina stresses and strains following the procedure described in Reference [22]. The lamina stresses and strains are applied in failure theories like maximum stress, maximum strain, Hoffman, Tsai-Hill and Tsai-Wu failure criterion to obtain first ply failure loads of the shell. The expressions of the failure theories are adopted from Reddy and Reddy [15]. The failure modes (in case of maximum stress and maximum strain failure criteria) and failure tendencies (in case of Hoffman, Tsai-Hill and Tsai-Wu failure criteria) are also identified using the steps elaborated in Reference [22].

2.2 *Delamination prediction*

Delamination at any interface between two adjacent laminae of the conoidal shell is predicted following the method adopted by Singh and Kumar [12]. The transverse normal stress (σ_3) and transverse shear stresses (τ_{13} and τ_{23}) are calculated at an interface and compared to their permissible values as given in Eq. (17). If the condition given in Eq. (17) satisfies then the delamination is considered to have occurred in a laminate.

$$\frac{\sigma_3}{Z_T} \geq 1 \text{ or } \frac{\tau_{13}}{R} \geq 1 \text{ or } \frac{\tau_{23}}{R} \geq 1 \tag{17}$$

σ_3 is calculated using Eq. (18).

$$\sigma_3 = C_{13} \times \varepsilon_1 + C_{23} \times \varepsilon_2 \tag{18}$$

$$C_{13} = E_{11}\frac{\nu_{31} + \nu_{21}\nu_{32}}{\Delta}, C_{23} = E_{22}\frac{\nu_{32} + \nu_{12}\nu_{31}}{\Delta}$$

$$\Delta = 1 - \nu_{12}\nu_{21} - \nu_{23}\nu_{32} - \nu_{13}\nu_{31} - 2\nu_{12}\nu_{23}\nu_{13}$$

The transverse shear stresses (τ_{13} and τ_{23}) are calculated using transverse shear strains in global axes (ε_{yz} and ε_{xz}) of the shell following Eq. (19).

$$\begin{Bmatrix} \tau_{23} \\ \tau_{13} \end{Bmatrix} = \begin{bmatrix} G_{23} & 0 \\ 0 & G_{13} \end{bmatrix} \begin{bmatrix} m & -n \\ n & m \end{bmatrix}^{-1} \begin{Bmatrix} \varepsilon_{yz} \\ \varepsilon_{xz} \end{Bmatrix} \tag{19}$$

$m = \cos\theta$ and $n = \sin\theta$. The elastic constants are given in Table 1.

Table 1. Material properties of Q-1115 graphite-epoxy composite.

Material constants			Permissible stresses			Permissible strains
E_{11}	142.50	GPa	X_T	2193.50	MPa $X_{\varepsilon t}$	0.01539
E_{22}	9.79	GPa	X_C	2457.0	MPa $X_{\varepsilon c}$	0.01724
E_{33}	9.79	GPa	Y_T=Z_T	41.30	MPa $Y_{\varepsilon t}$=$Z_{\varepsilon t}$	0.00412
G_{12}=G_{13}	4.72	GPa	Y_C=Z_C	206.80	MPa $Y_{\varepsilon c}$=$Z_{\varepsilon c}$	0.02112
G_{23}	1.192	GPa	R	61.28	MPa R_ε	0.05141
ν_{12} =ν_{13}	0.27		S	78.78	MPa S_ε	0.01669
ν_{23}	0.25		T	78.78	MPa T_ε	0.01669

3. Numerical problems

The non-dimensional static displacements of a spherical shell obtained from the proposed code are compared with closed form results reported by Reddy [26]. The comparison is reported in Table 2 with which the material properties and geometric dimensions of the shell are also furnished. Table 2 furnishes a convergence study to obtain the optimum finite element mesh. The study shows that an 8×8 mesh (8 divisions along each plan direction of the shell) shows converged static disdplacements. Table 2 confirms the correctness of the proposed finite element code as the present converged results are found in very good agreement with the closed form static displacements of the spherical shell.

The static bending formulation for the conoidal shell is found accurate when displacements of an isotropic shell calculated using the proposed code are in good agreement with the results reported by Hadid [27]. The comparison of displacements is furnished in Figure 3 where the dimensions and material properties of the shell are also reported. The nonlinear first ply failure loads of a partially clamped plate are calculated using the proposed code and found in close agreement with the experimental and theoretical results predicted by Kam *et al* [16]. The comparison of failure loads is reported in Table 3. Thus, it is confirmed that the geometrically nonlinear strains, calculation of lamina strains, lamina stresses and their application to different failure theories are correctly carried out in the proposed finite element code. The dimensions of the plate is furnished along with Table 3 and its elastic properties are reported in Table 1.

Once the accuracy of the proposed code is confirmed, it is further applied to study failure of laminated composite conoidal shell subjected to concentrated load at the centre. Two different boundary conditions (SSCC and CCSS) are adopted in this paper. The shell is taken as simply supported along $x = 0$ and $y = 0$ and clamped along $x = a$ and $y = b$ in SSCC boundary condition. The CCSS shell is taken

Table 2. Non-dimensional central displacements ($\hat{w}\times10^3$) of simply supported composite spherical shell under uniformly distributed load.

Lamination	0°/90°	0°/90°/0°	0°/90°/90°/0°
Reddy [26]	16.980	6.697	6.833
Present FEM (2 × 2)	8.294	5.116	4.644
4×4	16.898	6.724	6.820
6×6	16.969	6.710	6.826
(8×8)	17.009	6.707	6.835

$a/b = 1$, $a/h = 100$, $E_{11} = 25E_{22}$, $G_{12} = G_{13} = 0.5E_{22}$, $G_{23} = 0.2E_{22}$, $\nu = 0.25$, $E_{22} = 10^6$ N/cm^2, $R/a = 10^{30}$

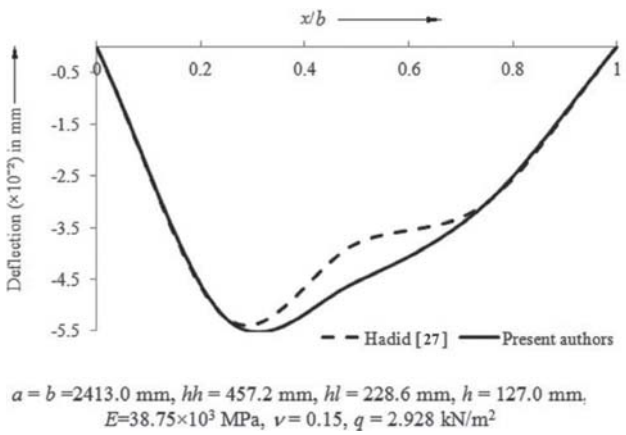

Figure 3. Comparison of static displacements of the isotropic conoid at $\frac{y}{a}$= 0.5.

as simply supported along $x = a$ and $y = b$ and clamped along $x = 0$ and $y = 0$. Both these boundary conditions have same number of degrees of freedom locked but arranged differently. Thus, the practicing civil engineers must be interested to explore the relative performances of both the shell options in order to achieve the maximum load carrying capacity against a fixed cost of fabrication. The dimensions of the conoidal shell is reported in Table 4. The

Table 4. Geometric dimensions of the shell.

Conoidal shell dimensions	Values	
Length (a)	1000	mm
Width (b)	1000	mm
Thickness (h)	10	mm
Higher height (hh)	200	mm
Lower height (hl)	50	mm

elastic constants and the permissible stresses and strains of the laminated composite material are furnished in Table 1.

Tables 5 and 6 report non-dimensional first ply failure loads, failure locations on the shell surface, the failed ply number and failure modes/tendencies for SSCC and CCSS boundary conditions, respectively. The ply number is counted from top of the laminate i.e. the topmost ply number is 1. The non-dimensional delamination failure load (load value at which delamination initiates within the laminate), failure location on the shell surface from where the delamination starts, failed interface and the transverse stress which initiates delamination are furnished in Table 7 for both the boundary conditions. Like, the ply numbers, the interfaces are also counted from the top of the laminate.

The first ply failure and delamination failure of the shell are studied for two and three layered laminates fabricated using symmetric and antisymmetric stacking sequences of cross and angle-ply laminations.

4. Results and discussion

The relative performance study of laminated composite conoidal shells in terms of non-dimensional first ply failure loads (FLD) from Tables 5 and 6 clearly show that among the arch directions of the conoid the deeper one should be clamped to obtain higher failure loads of cross-ply laminates and the shallower one should be clamped to maximize failure loads of angle-ply laminates. The non-dimensional delamination failure loads (DLD) reported in Table 7 also show similar relative behaviour of the shell where the

Table 3. Comparison of first ply failure loads in Newton for a $(0_2^0/90^0)_s$ plate.

Failure criteria	Side/ thickness	Theoretical failure loads (Kam *et al* [16])	Experimental failure load [16]	Failure loads (present code)
Maximum stress	105.26	147.61	157.34	135.94
Maximum strain		185.31		218.10
Hoffman		143.15		133.21
Tsai-Wu		144.42		134.50
Tsai-Hill		157.58		134.91

Note: Length = 100 mm, ply thickness = 0.155 mm, load details = central point load.

Table 5. First ply failure characteristics of laminated composite shell for SSCC condition.

Lamination (degree)	Failure theory	Non-dimensional failure load (FLD)	Location (x,y) (m,m)	First failed ply	Failure mode/failure tendency
0/90	Maximum stress	2.19×10^8	(0.5,0.38)	1	Transverse matrix cracking
	Maximum strain	2.12×10^8	(0.5,0.38)	1	Transverse matrix cracking
	Hoffman	$\mathbf{2.08 \times 10^8}$	(0.5,0.5)	2	Transverse matrix cracking
	Tsai-Hill	2.19×10^8	(0.5,0.38)	1	Transverse matrix cracking
	Tsai-Wu	2.17×10^8	(0.5,0.38)	1	Transverse matrix cracking
0/90/0	Maximum stress	2.86×10^8	(0.5,0.5)	3	Transverse matrix cracking
	Maximum strain	4.49×10^8	(0.5,0.5)	3	Transverse matrix cracking
	Hoffman	$\mathbf{2.54 \times 10^8}$	(0.5,0.5)	3	Transverse matrix cracking
	Tsai-Hill	2.67×10^8	(0.5,0.5)	3	Transverse matrix cracking
	Tsai-Wu	2.80×10^8	(0.5,0.5)	3	Transverse matrix cracking
45/-45	Maximum stress	9.80×10^7	(0.5,0.5)	2	Transverse matrix cracking
	Maximum strain	$\mathbf{8.93 \times 10^7}$	(0.5,0.5)	2	Transverse matrix cracking
	Hoffman	9.81×10^7	(0.5,0.5)	2	Transverse matrix cracking
	Tsai-Hill	9.77×10^7	(0.5,0.5)	2	Transverse matrix cracking
	Tsai-Wu	9.56×10^7	(0.5,0.5)	2	Transverse matrix cracking
45/-45/45	Maximum stress	1.74×10^8	(0.5,0.5)	3	Transverse matrix cracking
	Maximum strain	1.80×10^8	(0.5,0.5)	3	Transverse matrix cracking
	Hoffman	$\mathbf{1.73 \times 10^8}$	(0.5,0.5)	3	Transverse matrix cracking
	Tsai-Hill	1.73×10^8	(0.5,0.5)	3	Transverse matrix cracking
	Tsai-Wu	1.76×10^8	(0.5,0.5)	3	Transverse matrix cracking

deeper arch should be clamped for better performance of cross-ply laminates and the shallower one should be clamped for angle-ply laminates. An exception to this observation is noted where, for the Hoffman failure theory, the 0°/90° shell shows 0.42% higher first ply failure load for CCSS boundary than the failure load obtained for SSCC boundary. This marginally better performance of the CCSS shell over the SSCC one for cross-ply lamination does not defy the general observation that in order to achieve maximum utilization of the material strength the practicing engineers must choose the SSCC boundary for cross-ply shells and CCSS boundary for the angle-ply ones. It is interesting to observe that the relative performances of the shell largely depend on lamination and as a natural consequence the load carrying capacities vary widely for laminated conoids even though the material consumption is fixed. This means that for most effective utilization of the material different fiber orientations are to be tried to achieve the maximum benefit. Among different non-dimensional first ply failure loads for a given laminate corresponding to the five failure criteria reported in Tables 5 and 6, the engineering factor of safety should be applied to the minimum one to arrive at the working load of that laminate. The minimum FLD is highlighted in Tables 5 and 6 in bold letters. For a given boundary condition, the Hoffman failure criterion shows the minimum failure load for 0°/90° and 0°/90°/0° laminates. However, the antisymmetric angle-ply lamination (45°/− 45°) shows a different pattern where the maximum strain criterion yields the minimum failure load. Hoffman failure theory again yields the minimum load for symmetric 45°/-45°/45° laminate. It is noted that for cross and angle-ply laminations of both CCSS and SSCC shells, the first ply failure initiates when the normal stress perpendicular to fiber (σ_2) acting at middle of the bottommost lamina tend to exceed its permissible limit. The delamination failure, in contrast, does not initiate under the concentrated load. Table 7 shows that for a given lamination and boundary condition, the delamination is initiated through transverse normal stress (σ_3) acting at the bottommost interface of the conoidal shells.

Tables 5 and 6 also show that for a given boundary condition cross-ply laminations should be preferred over the angle-ply ones to fabricate the conoidal shell as the cross-ply laminates fail at higher magnitude of concentrated force than the failure loads of angle-ply laminates while the number of laminae in the laminate is kept constant. The non-dimensional delamination failure loads (Table 7) are also higher for the cross-ply shells than the failure loads of angle-ply ones. The conoidal shells in this study is supported along its four edges and subjected to transverse load. Thus, the shell deforms and transfers the governing forces and moments along its plan directions. The fibers of cross-ply laminations run along plan directions of the shell and hence, carry the governing stresses. In angle-ply laminations the fibers run along the diagonal directions of the shell. Thus, the governing stresses are carried by the matrix of angle-ply laminates. Since, the on-axis elastic modulus of a lamina is greater than its off-axis modulus the cross-ply shells fail at higher load compared to the angle-ply ones.

Table 6. First ply failure characteristics of laminated composite shell for CCSS condition.

Lamination (degree)	Failure theory	Non-dimensional failure load (FLD)	Location (x,y) (m,m)	First failed ply	Failure mode/failure tendency
0/90	Maximum stress	2.18×10^8	(0.5,0.5)	1	Transverse matrix cracking
	Maximum strain	2.12×10^8	(0.5,0.63)	1	Transverse matrix cracking
	Hoffman	$\mathbf{2.09 \times 10^8}$	(0.5,0.5)	2	Transverse matrix cracking
	Tsai-Hill	2.18×10^8	(0.5,0.63)	1	Transverse matrix cracking
	Tsai-Wu	2.16×10^8	(0.5,0.63)	1	Transverse matrix cracking
0/90/0	Maximum stress	2.85×10^8	(0.5,0.5)	3	Transverse matrix cracking
	Maximum strain	4.41×10^8	(0.5,0.5)	3	Transverse matrix cracking
	Hoffman	$\mathbf{2.54 \times 10^8}$	(0.5,0.5)	3	Transverse matrix cracking
	Tsai-Hill	2.67×10^8	(0.5,0.5)	3	Transverse matrix cracking
	Tsai-Wu	2.79×10^8	(0.5,0.5)	3	Transverse matrix cracking
45/-45	Maximum stress	9.95×10^7	(0.5,0.5)	2	Transverse matrix cracking
	Maximum strain	$\mathbf{9.08 \times 10^7}$	(0.5,0.5)	2	Transverse matrix cracking
	Hoffman	9.95×10^7	(0.5,0.5)	2	Transverse matrix cracking
	Tsai-Hill	9.92×10^7	(0.5,0.5)	2	Transverse matrix cracking
	Tsai-Wu	9.71×10^7	(0.5,0.5)	2	Transverse matrix cracking
45/-45/45	Maximum stress	1.74×10^8	(0.5,0.5)	3	Transverse matrix cracking
	Maximum strain	1.80×10^8	(0.5,0.5)	3	Transverse matrix cracking
	Hoffman	$\mathbf{1.73 \times 10^8}$	(0.5,0.5)	3	Transverse matrix cracking
	Tsai-Hill	1.74×10^8	(0.5,0.5)	3	Transverse matrix cracking
	Tsai-Wu	1.76×10^8	(0.5,0.5)	3	Transverse matrix cracking

Table 7. Delamination characteristics of the laminated composite shell.

Lamination (degree)	Boundary condition	Non-dimensional failure load (DLD)	Location (x,y) (m,m)	Failed interface	Failure stress
0/90	SSCC	3.99×10^8	(0.5,0.38)	1	Transverse normal stress
	CCSS	3.87×10^8	(0.5,0.63)	1	Transverse normal stress
0/90/0	SSCC	6.82×10^8	(0.56,0.5)	2	Transverse normal stress
	CCSS	6.73×10^8	(0.56,0.5)	2	Transverse normal stress
45/-45	SSCC	2.94×10^8	(0.5,0.38)	1	Transverse normal stress
	CCSS	3.33×10^8	(0.5,0.63)	1	Transverse normal stress
45/-45/45	SSCC	4.24×10^8	(0.5,0.38)	2	Transverse normal stress
	CCSS	4.61×10^8	(0.5,0.38)	2	Transverse normal stress

The symmetric stacking sequences of cross and angle-ply laminations show higher non-dimensional first ply failure and delamination failure loads than their antisymmetric counterparts. The reduction in bending-stretching coupling for the symmetric laminates can be attributed to the fact. Among all the shell options taken up here, the 0°/90°/0° laminate shows the best performance by exhibiting the highest non-dimensional first ply failure and delamination failure loads considering both SSCC and CCSS boundary conditions.

It is interesting to note from Tables 5, 6 and 7 that the first ply failure precedes delamination for a conoidal shell keeping its boundary condition and lamination fixed. Among the cross-ply laminations, the symmetric 0°/90°/0° one shows the highest difference between the first ply failure and delamination failure loads. The 45°/− 45° shell shows the highest difference between failure loads when the comparison is restricted within angle-ply laminations. Since the delamination failure load is atleast 85% greater than the governing first ply failure load (the minimum failure load) of a laminate, the first ply failure load can be taken up as the load carrying capacity of the shell on which the engineering factor of safety should be applied to obtain the working load. The working load is designated as the load value corresponding to the serviceable displacement of the shell which is taken as span/250 = 4 mm in this study. The displacements at failure for the conoid is furnished in Table 8 corresponding to all the laminates considered here.

Table 8 shows that displacement at failure is within the permissible limit for 45°/− 45° laminate only. The displacements at failure for the other shell options have exceeded the permissible limit. Thus, the working load values for all the laminates are reported in Table 8. For a given laminate, the factor of safety (FOS) values are

Table 8. FOS applicable to obtain the working loads.

Lamination (degree)	Displacement at first ply failure (mm)	Non-dimensional working load	FOS
0/90	8.357	9.94×10^7	2.09
0/90/0	5.899	1.72×10^8	1.47
45/-45	3.039	1.18×10^8	0.76
45/-45/45	4.186	1.65×10^8	1.05

obtained by dividing the non-dimensional first ply failure loads with their non-dimensional working loads. The FOS values are also furnished in Table 8. Since the FOS values are provided in design codes of practices as integers or half the integers, a FOS 2.50 is recommended for all the shell options taken up in this study.

5. Conclusions

The following conclusions can be drawn from the present study.

(a) The proposed finite element code is capable to accurately predict first ply failure and delamination failure of laminated composite conoidal shells as it was established by solution of the benchmark problems.
(b) The relative performance study of CCSS and SSCC conoidal shells reveals that the practicing civil engineers must adopt the SSCC boundary for cross-ply shells and CCSS boundary for the angle-ply ones.
(c) The present study on conoidal shells shows that the cross-ply laminations offer greater load carrying capacity than the angle-ply ones and the practicing engineers are recommended to adopt the 0°/90°/0° lamination to fabricate the conoidal shell as it exhibits the best performance in terms of first ply failure and delamination failure loads.
(d) All the shell options taken up here fail through the bottommost lamina and under the load point. Thus, a set of concentric stiffeners along both plan directions may be provided at the bottom of the shells to enhance their failure load values.

Acknowledgement

This paper is a revised and expanded version of an article entitled, "Relative Performance Study of Composite Conoidal Shell Roofs in Terms of First Ply Failure Loads", Paper No., "054" presented in "First International Conference on Mechanical Engineering" held at 'Jadavpur University', Kolkata, India during January 4–6, 2018.

Abbreviations

a, b	Length and width of shell
DLD	Non-dimensional delamination failure load $=(D/E_{22})(a/h)^4]$
D	Delamination failure load in Newton
E_{11}, E_{22}, E_{33}	Elastic moduli
FLD	Non-dimensional first ply failure load = $(F/E_{22})(a/h)^4$
F	First ply failure load in Newton
G_{12},G_{13}, G_{23}	Shear moduli
h	Shell thickness
ne	Number of elements
$\{q\}$	Lumped load vector containing the scalar point load value at the central node acting parallel to the negative 'z' axis
R	Radius of spherical shell
T	Shear strength of lamina
T_ε	Allowable shear strain of lamina
$\hat{w}$	Non-dimensional displacement = $wE_{22}h^3/(qa^4)$
X_T, X_C	Normal strengths of lamina
$X_{\varepsilon T}$, $X_{\varepsilon C}$	Allowable normal strains of lamina
Y_T, Y_C	Normal strengths of matrix
$Y_{\varepsilon T}$, $Y_{\varepsilon C}$	Allowable normal strains of matrix
v_{ij}	Poisson's ratio

References

[1] Das H S and Chakravorty D 2007 Design aids and selection guidelines for composite conoidal shell roofs—a finite element application. *J. Reinf. Plast. Compos*., 26: 1793–1819
[2] Das H S and Chakravorty D 2011 Bending analysis of stiffened composite conoidal shell roofs through finite element application. *J. Compos. Mater*. 45: 525–542
[3] Das H S and Chakravorty D 2008 Natural frequencies and mode shapes of composite conoids with complicated boundary conditions. *J. Reinf. Plast. Compos*. 27: 1397–1415
[4] Das H S and Chakravorty D 2009 Composite full conoidal shell roofs under free vibration. *Adv. Vib. Eng*. 8: 303–310
[5] Kumari S and Chakravorty D 2010 On the bending characteristics of damaged composite conoidal shells—a finite element approach. *J. Reinf. Plast. Compos.* 29: 3287–3296

[6] Kumari S and Chakravorty D 2011 Bending of delaminated composite conoidal shells under uniformly distributed load. *J. Eng. Mech.-ASCE*, 137: 660–668

[7] Nayak A N and Bandopadhyay J N 2006 Dynamic response analysis of stiffened conoidal shells. *J. Sound. Vib*. 291: 1288–1297

[8] Pradyumna S and Bandyopadhyay J N 2008 Static and free vibration analyses of laminated shells using a higher-order theory. *J. Reinf. Plast. Compos*. 27: 167–186

[9] Pradyumna S and Bandyopadhyay J N 2011 Dynamic instability behaviour of laminated hypar and conoid shells using a higher-order shear deformation theory. *Thin-Walled Struct*. 49: 77–84.

[10] Chaubey A K, Kumar A and Chakrabarti A 2018 Novel shear deformation model for moderately thick and deep laminated composite conoidal shell. *Mech. Based Des. Struct*. 46: 650–668

[11] Chaubey A, Kumar A, Fic S, Hunek D B, Buraczewska BS 2019 Hygrothermal analysis of laminated composite skew conoids. *Materials*, 12: 225

[12] Singh S B and Kumar A 1998 Postbuckling response and failure of symmetric laminates under in-plane shear. *Compos. Sci. Technol*. 58: 1949–1960

[13] Akhras G and Li W C 2007 Progressive failure analysis of thick composite plates using the spline finite strip method. *Compos. Struct*. 79: 34–43.

[14] Ganesan R and Liu D Y 2008 Progressive failure and post–buckling response of tapered composite plates under uni–axial compression. *Compos. Struct*. 82: 159–176

[15] Reddy Y N S and Reddy J N 1992 Linear and nonlinear failure analysis of composite laminates with transverse shear. *Compos. Sci. Technol*. 44: 227–255

[16] Kam T Y, Sher H F, Chao T M and Chang R R 1996 Predictions of deflection and first ply failure load of thin laminated composite plates via the finite element approach. *Int. J. Solids. Struct*. 33: 375–398

[17] Lal A, Singh B N and Patel D 2012 Stochastic nonlinear failure analysis of laminated composite plates under compressive transverse loading. *Compos. Struct*. 94: 1211–1223

[18] Prusty B G, Satsangi S K and Ray C 2001 First ply failure analysis of stiffened panels - a finite element approach. *Compos. Struct*. 51: 73–81

[19] Sengupta J, Ghosh A and Chakravorty D 2015 Progressive failure analysis of laminated composite cylindrical shell roofs. *J. Fail. Anal. Preven.* 15: 390–400

[20] Ghosh A and Chakravorty D 2017 Failure analysis of civil engineering composite shell roofs. *Procedia Eng*. 173: 1642–1649

[21] Ghosh A and Chakravorty D 2018 First-ply-failure performance of composite clamped spherical shells. *Mech. Compos. Mater.* 54: 191–206

[22] Bakshi K and Chakravorty D 2015 First ply failure loads of composite conoidal shell roofs with varying lamination. *Mechanics of Adv. Mater. Struct.* 22: 978–987

[23] Bakshi K and Chakravorty D 2017 Geometrically nonlinear first ply failure loads of laminated composite conoidal shells. *Procedia Eng.* 173: 1619–1626

[24] Sanders J L 1963 Nonlinear theories for thin shells. *Quart. Appl. Math*. 21: 21–36

[25] Chattopadhyay B, Sinha P K and Mukhopadhyay M 1995 Geometrically nonlinear analysis of composite stiffened plates using finite elements. *Compos. Struct.* 31: 107–118

[26] Reddy JN 1984 Exact solutions of moderately thick laminated shells. *J. Eng. Mech.-ASCE*. 110: 794 – 809

[27] Hadid H A 1964 *An analytical and experimental investigation into the bending theory of elastic conoidal shells*, Ph.D. Thesis, University of Southampton, United Kingdom